National Aeronautics and Space Administration

Orbital Debris Quarterly News

Volume 29, Issue 2
May 2025

Inside...

A publication of the NASA Orbital Debris Program Office (ODPO)

ISS Maneuvers Twice to Avoid Debris

The International Space Station (ISS) conducted two Pre-planned Debris Avoidance Maneuvers (PDAMs) to mitigate high-risk conjunctions with two different fragmentation debris in November 2024. The first PDAM took place at 3:24 GMT on 19 November 2024. The avoided object (International Designator 1995-015FU, U.S. Satellite Catalog Number 40680) was a fragment generated from the accidental explosion of a Defense Meteorological Satellite Program (DMSP) 5D-2 F13 spacecraft in 2015 (ODQN, vol. 19, issue 2, April 2015, pp. 1-2). Less than a week later, at 3:30 GMT on 25 November 2024, the ISS conducted another PDAM. The target this time was a different fragment (International Designator 1999-025AEN, U.S. Satellite Catalog Number 30423), which was generated from the *Fengyun-1C* (*FY-1C*) anti-satellite test conducted by China in 2007 (ODQN, vol. 11, issue 2, April 2007, pp. 2-3). These two PDAMs increased the total number of collision avoidance maneuvers conducted by the ISS to mitigate high-risk conjunctions with objects tracked by the Space Surveillance Network (SSN) to a total of 40 since 1999.

The frequency of the avoidance maneuvers is affected by the number of tracked objects crossing the ISS orbit, tracking capability and tasking of the SSN, solar activity, and other factors. Nevertheless, there is a strong correlation between the frequency and solar activity, as shown in the Figure. The current Solar Cycle 25 is predicted to reach its maximum in 2025. If the historical trend continues, fewer ISS PDAMs are expected in the coming years as solar activity moves toward its next minimum. ♦

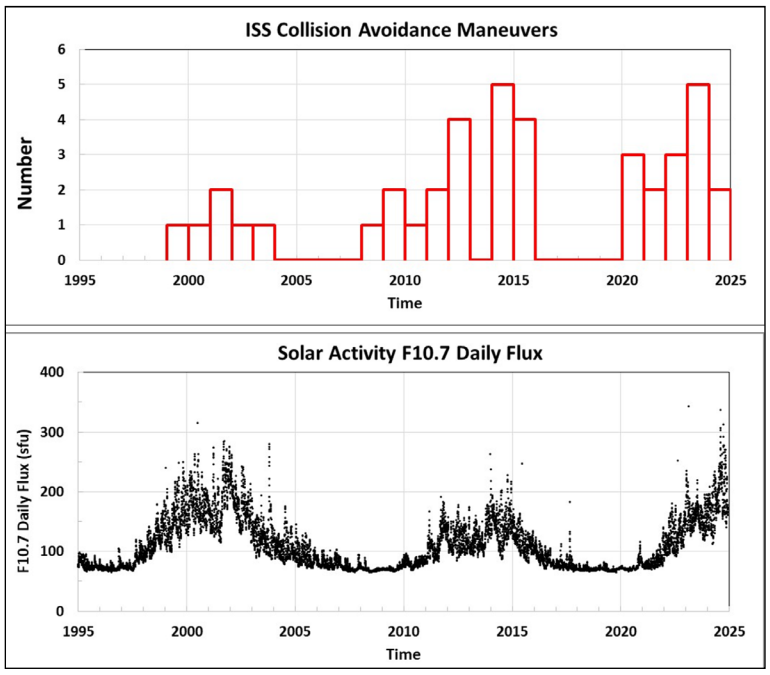

PROJECT REVIEWS

Python Scripting API for the Debris Assessment Software

GREENE, B., OPIELA, J., OSTROM, C.

The NASA Debris Assessment Software (DAS) provides assessments that can verify compliance of a spacecraft, upper stage, and/or payload with NASA's requirements for limiting debris generation, spacecraft vulnerability, post-mission lifetime, and entry safety, as enumerated in NASA Technical Standard 8719.14C. The NASA Technology Transfer Program reports that DAS is consistently at or near the top three of the list of most-downloaded software titles (followed closely by the Orbital Debris Engineering Model [ORDEM]). The upcoming version 3.2.7 release of DAS will include several bug fixes and a new Python scripting application programming interface (API) for automating many of the commonly used features of DAS without needing to interact with the graphical user interface. This project review will summarize the Python API interface with DAS and the types of automation scripting available for DAS projects. The DAS installation will also include sample scripts for each available subroutine. These sample scripts have been tested with Windows 10/11 and Python 3.8 and higher.

The new DAS Python API uses the *ctypes* library, part of the standard Python installation, to interface with the dynamically linked library (DLL) file located in the DAS installation directory that provides the core DAS functions. Through the API, the user can access:

- calculation of the apogee/perigee history,
- orbit lifetime/dwell time prediction,
- calculation of spacecraft cross-sectional area,
- large object collision probability (Requirement 4.5-1),
- small object collision probability (Requirement 4.5-2),
- postmission disposal compliance (Requirement 4.6-1 to 4.6-3), and
- reentry human casualty risk (Requirement 4.7-1).

The API consists of the names of the subroutines included in the DLL file and descriptions of their input and output variables and variable types. A full description of the API will be provided in the DAS 3.2.7 User's Guide, but a sample of the input and output variables for the reentry casualty risk assessment subroutine, "MORSAT," is shown in the Table.

continued on page 3

Table. Input and Output Variables in MORSAT subroutine.

Variable	Intent	Python type(s)	Fortran type	Description
strTmpPath	input	str	character(*)	Project folder file path
inc	input	float	real(8)	Orbit inclination angle (deg)
ncomp	input	int	integer(4)	Total number of components
parent	input	numpy array	integer(4), dimension(ncomp)	The row number of the parent object of each object
qty	input	numpy array	integer(4), dimension(ncomp)	Quantity of each object
imat	input	numpy array	integer(4), dimension(ncomp)	Material ID # for each object
itype	input	numpy array	integer(4), dimension(ncomp)	Shape type for each object: 1 – sphere, 2 – cylinder, 3 – flat plate, 4 – box
amass	input	numpy array	real(8), dimension(ncomp)	Aerodynamic mass for each object
shape	input	numpy array	real(8), dimension(ncomp,4)	Modeling parameters for each object where shape(i, 1) is thermal mass (kg), shape(i,2) is diameter/width (m), shape(i,3) is length (m), and shape(i,4) is height (m)
entryYear	input	int	integer(4)	Entry year
hd	output	numpy array	real(8), dimension(ncomp)	Demise altitude for each object (m)
dca	output	numpy array	real(8), dimension(ncomp)	Debris casualty area for each object (m^2)
KE	output	numpy array	real(8), dimension(ncomp)	Impact kinetic energy of each object (J)
ilenTmpPath	input	int	integer(4)	Length of strTmpPath
Ec	output	float	real(8)	Expectation of casualty for the parent object
sumdca	output	float	real(8)	Total DCA for all objects

Python Scripting

continued from page 2

The Figure shows the program flow and steps needed to interact with DAS subroutines through the scripting API. Importing libraries and connecting to the DAS DLL file need to be performed only once, and then the subroutine may be called as many times as necessary within the script.

The example scripts supplied with the DAS 3.2.7 installation encapsulate the calls to the DAS subroutines and all the steps detailed in the Figure within Python functions, allowing the script files to be added to any Python project folder and the function imported into the user's own script using the Python *import* statement. The imported function can then be called like any other Python function, accepts data in native Python data types, and provides results in native Python data types. This provides an easy way to incorporate DAS subroutines into an automation script; the only required edit to the example script is to change the DAS installation directory defined in the code to the one on the target machine. The scripts themselves have been commented to explain the function of each part of the code so if a more tailored implementation is needed, the user will have the information needed to alter the script to their own needs.

One of the primary uses for the Python scripting interface is to provide a range of values to the DAS subroutines to perform trade studies or parametric design tasks. Multiple calls to a subroutine may be performed serially within a script or in parallel using Python's *multiprocessing* library. All subroutines provide the primary results of the calculations to the specified output variables, which can then be directly used in other calculations within the script.

Care should be taken with some of the subroutines when providing multiple different inputs to the same routine within a script. Some of the subroutines, including the reentry human casualty risk calculation, require a path to a project folder be provided. This folder may be used to write temporary files, output files, or read further data inputs, so it is important for this folder to contain the expected files and that those files are consistent with the inputs provided through the scripting interface or the subroutine may return unexpected results.

In the case of the reentry human casualty risk calculation, the file defining the properties of user-defined materials is stored in the specified project folder. Collision risk assessments use this folder to write ORDEM input files. For the cross-sectional area calculation subroutine, the detailed output files are written to this folder.

The subroutines for calculating the orbit lifetime, large object collision probability, and post-mission disposal compliance use scalar inputs and outputs, and so these require only the standard Python installation. For the other routines, arrays of values must be passed between the Python script and the Fortran subroutines, which requires the third-party *numpy* library. This library is free open-source software provided under a modified BSD license. More information about the library and how to download it is available at numpy.org.

The new Python scripting API in DAS 3.2.7 will provide powerful new tools for spacecraft operators and designers to automate their debris assessments. This will make it easier to run multiple design trade scenarios, streamline assessments of updated designs, and allow operators and designers to optimize their contribution and response to the space debris environment. ♦

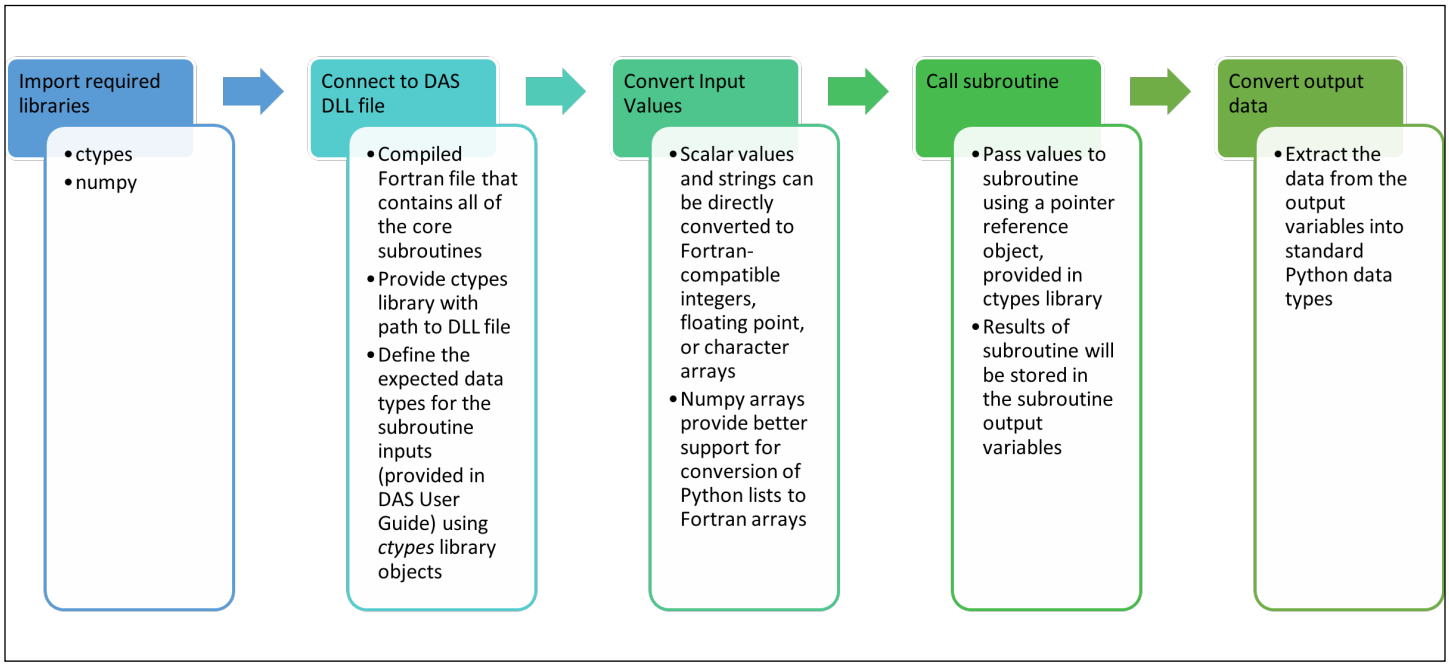

Figure. Steps to connect to and call a subroutine through the DAS Python scripting API.

Recovered SpaceX Dragon Trunk Reentry Fragment Study

DOUGHERTY, A., GREENE, B., OSTROM, C.

On 8 July 2022, the trunk section from the SpaceX Dragon Crew-1 mission reentered over New South Wales, Australia, and over the following month, several fragments were recovered. One of the surviving fragments located was a portion of the trunk, constructed largely of carbon fiber-reinforced polymer (CFRP) composite, a material that has garnered profound interest from the space safety community in recent years due to the nature of the material to not completely demise upon reentry (ODQN vol. 28, issue 4, pp. 3-5; ODQN vol. 24, issue 2, pp. 5-6). Working with SpaceX and the Australian Space Agency, the NASA Orbital Debris Program Office (ODPO) obtained a 1 m x 1 m recovered fragment from the forward end of the Dragon Crew-1 trunk to characterize the extent of the reentry damage experienced by the fragment and compare it to reentry model predictions. All analyses for the fragment are being acquired with the ODPO's Fragment Analysis Facility, which features several analytical instruments to support material and target inspections on-site at Johnson Space Center (ODQN vol. 28, issue 1, pp. 5-8).

Phase I of the study focuses on surface characterization using microscopy and laser ablation element analysis. Thirty-two sites of interest have been identified for study (Figure 1). These sites include exposed but unpyrolized carbon fiber/epoxy composite, pyrolized composite, thermal protection material, melted metal surfaces, and fractured metal surfaces. Microscope observations performed for the pyrolized and unpyrolized composite surfaces show a striking variability in degree of charring, indicative of extended periods of protection of some parts of the trunk structure from reentry heating.

The ODPO safety team uses a variable zoom lens (x20-200) to take wide images (x20) of the sites of interest and identify locations for higher magnification images (x100-200) and depth compositions. The microscope head is mounted on a mobile medical equipment arm to suspend it above the surface of the fragment while still allowing ease of movement between the sites (ODQN vol. 28, issue 1, p. 8). The position of each image location is cataloged using an X-Y coordinate system with the origin at the bolt hole near the center of the outer surface (at the corner of the carpenter's square in Figure 1, as marked by the blue cross). The images collected so far provide a glimpse into the conditions faced by the trunk materials during reentry.

The initial work had focused on the sites of interest located on the outer surface of the fragment. These sites are predominantly exposed carbon fiber/epoxy composite structural material that has been pyrolized, melted, or vaporized to varying degrees. Figure 2 shows partially charred carbon fiber composite from Sites 5 and 6, and charred resin matrix residue on two aluminum mounting inserts, one each at Sites 7 and 8, integrated into the CFRP layup.

The CFRP layup on the outer fragment surface has visual markers to suggest highly and unevenly charred surfaces, as can be seen in Figure 2a (top left), where the degree of matrix removal varies widely within the width of a few fiber bundles (4-6 mm). In the higher magnification image of Site 6 in Figure 2b (top right), near-complete matrix removal from the first couple layers of CFRP fabric is evident. Both Sites 5 and 6 are located at the edges of the fragment. It is instructive to compare the degree of charring at these sites to the relatively thin residue of resin matrix on the aluminum surfaces at Sites 7 and 8 in Figure 2c (bottom left) and 2d (bottom right), respectively. The sites closer to the center of the fragment display significantly less matrix removal than those close to where the fragment broke off the main structure. This seems to indicate that this section of the outer surface of the trunk was shielded from the highest heat flux until breakup of the main structure, and even then, faced predominantly into the leeward

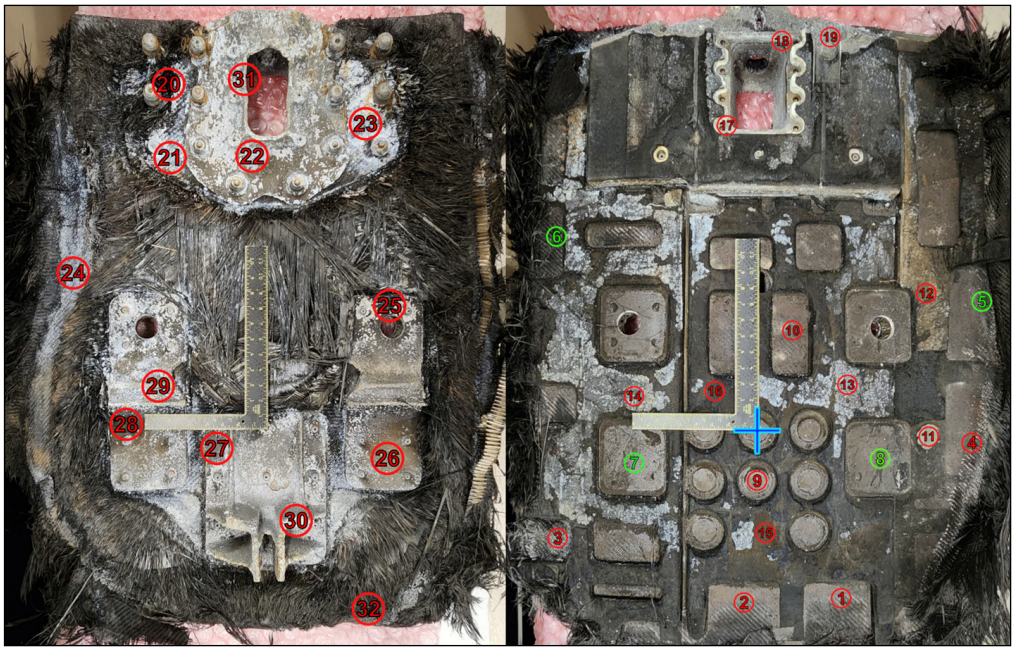

Figure 1. Inner (left) and outer (right) faces of the fragment with the location of each site of interest indicated in red and green. The green circles indicate samples already under study/analysis. Images from the sites marked in green are shown in Figure 2.

continued on page 5

Reentry Study

continued from page 4

flow such that only the edges absorbed significant heat.

The thickness of residual deposits of charred matrix material are optically measured using image stacking. Figure 3 shows a side-by-side comparison of a true-color depth-mapped image of a region in Site 4 and a false-color image showing the depth measurement. This region of the site contains a gouge in the residue that can provide an estimate of the residue thickness without the need for destructive tests at this early stage. These measurements show this char residue is approximately 0.6 mm thick on the surface of the fiber weave.

Several preliminary conclusions can be drawn about the reentry environment experienced by the Dragon Crew-1 trunk using initial microscope measurements. Primarily, given the large difference in charring on the inside versus the outside surface, it seems that the trunk was not tumbling significantly during most of the reentry, and even after breakup, the recovered fragment seems to have had a relatively stable attitude at least during the peak heating period.

Further measurements of metal grain structure, fracture surfaces, and residual material strength will inform future conclusions, including the nature of the separation of the metal components from the CFRP structure and the peak temperature experienced by different areas of the fragment. This will provide insight into the reentry breakup and demise process for structures composed predominantly of carbon fiber/epoxy and carbon fiber/phenolic composite materials and validate computational models for reentry human casualty risk from modern orbital debris as mentioned herein. ♦

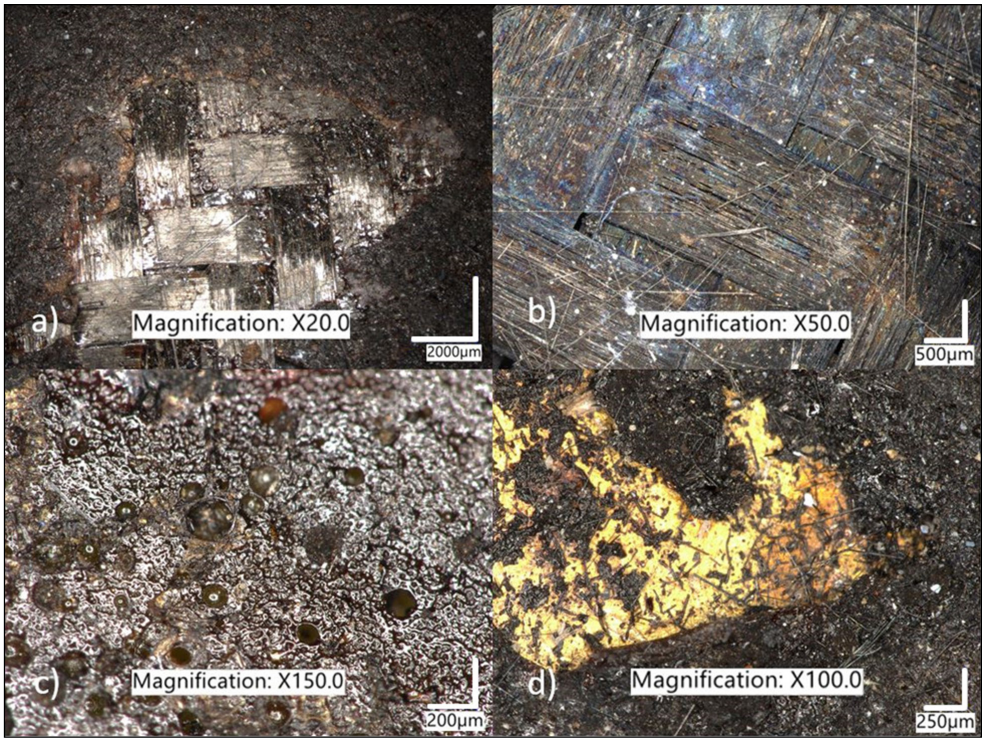

Figure 2. Microscope images from the outer surface of the fragment showing varying levels of resin matrix charring within a relatively small area in four different sites of interest: a) Site 5, 20x magnification; b) Site 6, 50x magnification; c) Site 7, 150x magnification; d) Site 8, 100x magnification.

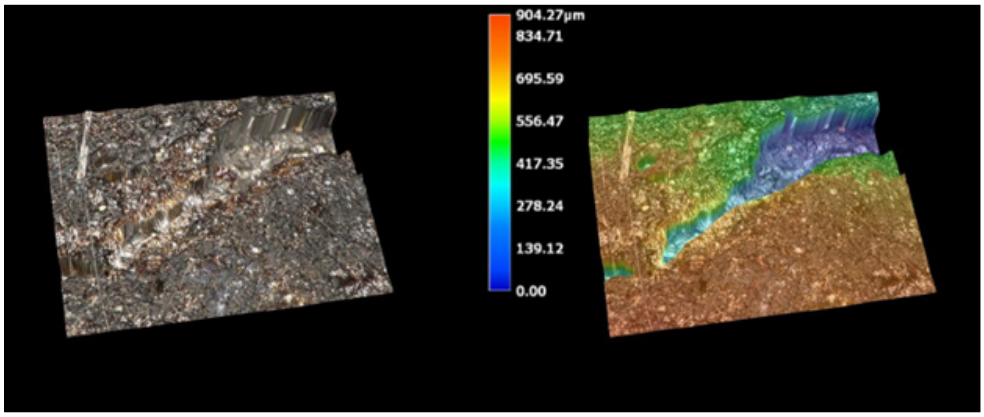

Figure 3. Side-by-side comparison of depth composition with and without height coloring at Site 4.

Subscribe to the ODQN or Update Your Subscription Information

To be notified by email when a new issue of the ODQN is placed online, or to update your personal information, please navigate to the ODQN subscription page on the NASA Orbital Debris Program Office (ODPO) website at: https://orbitaldebris.jsc.nasa.gov/quarterly-news/subscription.cfm. The ODPO respects your privacy. Your email address will be used solely for communication from the ODQN Managing Editor.

MEETING REPORTS

4-6 February 2025: 6th Annual VOLTRON Meeting, Albuquerque, New Mexico, USA

The 6th Annual VOLTRON meeting was hosted by the Air Force Research Laboratory (AFRL). VOLTRON focuses on laboratory and observational techniques for improving space situational awareness. The aim is to provide a forum for discussion of photometric and spectroscopic observations of artificial space objects and how laboratory measurements can support analysis of these observations. Meeting participants included researchers from academia, industry, government, and federally funded research and development centers. Topics covered in the program were space object observation and characterization; optical and radar techniques for orbital debris; satellite material modeling; innovations in photometric and spectral analyses for GEO satellites; and frontiers in spacecraft material interactions and resilience.

This year's meeting featured a classified session, helping improve the total number of attendees to over 100. A total of 28 oral and 6 poster presentations were given, including 2 presentations from the Orbital Debris Program Office (ODPO) on optical and radar laboratory measurements. First, "A Historical Overview of the NASA Orbital Debris Program Office's Laboratory Optical Measurements," which provided a broad retrospective of optical photometric and spectroscopic studies carried out by the ODPO on various materials and targets such as hypervelocity impact experiment fragments and rocket body models, as well as naturally and experimentally space weathered materials. These measurements provide a better understanding of the optical and *in situ* measurements that underlie the ODPO's environmental models. The second paper presented was titled "Laboratory Radar Measurements in Support of the NASA Orbital Debris Program Office's Size Estimation Model," which discussed results of a compact radar range study of calibration targets designed to assess the sensitivity of laboratory measurements to objects with sizes, shapes, and materials common to debris fragments. The VOLTRON organizing committee is working on plans for the next host for the 7th annual VOLTRON expected to occur in February 2026. ♦

1-4 April 2025: 9th European Conference on Space Debris, Bonn, Germany

The 9th European Conference on Space Debris was held 1-4 April 2025 in Bonn, Germany. This latest edition of the quadrennial conference was a forum for information exchange, technical discussions, and networking between researchers, engineers, and decision-makers from 32 countries representing academia, government, and industry. Approximately 500 subject matter experts from around the world participated in this major event. The full program can be accessed at https://space-debris-conference.sdo.esoc.esa.int/page/programme.

The 4-day conference comprised 26 sessions with 148 oral presentations and 92 posters, covering topics such as: radar measurements; optical measurements; economics and policy; reentry risk; reentry observations; space traffic coordination; lunar space debris issues; active debris removal; environmental modeling; hypervelocity impact risk; environment capacity and uncertainty; decommissioning and post-mission disposal; attitude dynamics; and space debris missions and products. Each day of the conference also featured a panel session. Day 1's panel "How can we accelerate mitigation technologies maturation?" covered the increased usage of Earth orbits, the lagging compliance with debris mitigation guidelines, and means for improving the implementation of mitigation technologies. The panel on Day 2, "How re-entry strategies can balance safety and sustainability towards a zero-impact future," discussed developments in design for demise, measurements of satellite materials in atmospheric aerosols, and future challenges in mitigating the effects of reentering objects on the environment. The panel on Day 3, "From Data to Decision: open points for scalable space traffic coordination architectures," focused on the new governmental and commercial services and the maturity of space surveillance products and the potential for space traffic coordination. The final panel on Day 4, "Why is cislunar debris a concern?," covered the challenges in detecting, tracking, cataloging, and mitigating debris in the cislunar regime.

Representatives from the NASA Orbital Debris Program Office (ODPO) served on the conference program committee, co-chaired two of these technical sessions, participated in one panel session, and presented eight papers, including: a comparison of four space agencies' reentry simulation tools; an update on breakup models using the DebriSat project data; a summary of the Eugene Stansbery Meter Class Autonomous Telescope (ES-MCAT) GEO surveys conducted from 2020-2023 and machine learning techniques to improve detection performance; a study on the effects of long-duration exposure to atomic oxygen on thin polyimides; results of laboratory radar cross section measurements of common aerospace materials; a summary of radar observations from 2016-2023 using the Haystack Ultrawideband Satellite Imaging Radar (HUSIR) and Goldstone Orbital Debris Radar; a development status update on the latest Orbital Debris Engineering Model (ORDEM 4.0); and a summary of the Multilayer Acoustic & Conductive Grid Sensor (MACS) technology development and its upcoming demonstration mission on HTV-X3. In addition, the JSC Hypervelocity Impact Technology team also presented two papers on the risks to the International Space Station from micrometeoroids and orbital debris, and an exploration of how basalt fabric performs as a substitute material in stuffed Whipple and multishock shields. A Program Executive from NASA's Science Mission Directorate also presented a paper on orbital debris and space situational awareness activities in NASA's Heliophysics Division. Papers and posters from the conference can be accessed from the conference proceedings database at https://conference.sdo.esoc.esa.int/proceedings/list. ♦

CONFERENCE ABSTRACTS FROM THE NASA ODPO

The 9th European Conference on Space Debris, 1-4 April 2025, Bonn, Germany

Authors	Abstract Title and Summary
C. OSTROM, J. ANNALORO, K. SATO, T. LIPS, B. GREENE, E. CONSTANT, *ET AL.*	***Comparison of CNES, ESA, JAXA, and NASA Reentry Analysis Tools — Phase I: Model Descriptions and Survivability of Individual Components*** This paper presents the main results of PAMPERO, DEBRISK, SCARAB, DRAMA, ORSAT, and ORSAT-J for the simple shape case and addresses the sources of discovered differences. Discussion of the results of previous comparisons is made for a summary of differences between the codes and lessons learned from this series of tests.
H. COWARDIN, M. MATNEY, M. SORGE, D. MAINS, P. ANZ-MEADOR, *ET AL.*	***DEBRISAT Updates via NASA's SSBM and DOD's IMPACT Breakup Model*** This paper will provide an overview of the DebriSat project; background on SSBM and IMPACT; a comparison of DebriSat fragment distributions to both breakup models; and a discussion of the similarities, differences, and future development of each model.
C. CRUZ, B. BUCKALEW, J. MELO, M. LAMBERT, AND A. MANIS	***Detection and Analysis Techniques for Optical Telescope Data and Machine Learning Applications*** This paper provides an overview of ES-MCAT GEO survey strategies, including updates made from the first to the second GEO survey; a summary of data collected during the first and second ES-MCAT GEO surveys and comparisons to historical MODEST data; and a discussion of performance of ML models implemented with ES-MCAT data.
E. PLIS, R. RAMIREZ, A. SEMENOVA, D. HEWETT, D. OAKES, AND H. COWARDIN	***Long-duration Experiments Assessing Atomic Oxygen Effects on Thin Polyimides*** This study involves long-duration experiments to evaluate the effects of AO on various types of thin polymer films.
J. A. HEADSTREAM, A. MANIS, M. MATNEY, AND M. MAGALETTA	***Measuring Radar Cross Section of Common Spacecraft Materials*** Results of these laboratory RCS measurements will be presented as charts of azimuthal RCS and RCS versus frequency and will include comparisons with computational models for selected samples. The application of laboratory RCS measurements to orbital debris radar data will also be discussed, particularly comparing the circular polarization behavior of conductive versus dielectric materials. The paper will then outline the next steps for choosing representative DebriSat fragments for laboratory RCS measurements that will contribute to the planned update to the NASA SEM.
A. MANIS, J. A. HEADSTREAM, M. POEHLMANN, P. ANZ-MEADOR, AND M. MATNEY	***Monitoring the Small Debris Environment with Ground-based Radar: An Assessment of Data from 2016-2023*** This paper provides a summary of HUSIR and Goldstone observations of debris below the size threshold of the SSN and their temporal evolution from 2016 through 2023. Specific debris-generating events are analyzed further, including the debris clouds from major collisions and explosions, the special sodium-potassium (NaK) population at approximately 65° inclination, and a persistent debris cloud evident at approximately 82° inclination.
M. MATNEY, A. VAVRIN, M. POEHLMANN, A. KING, J. SEAGO, *ET AL.*	***ORDEM 4.0: NASA's Orbital Debris Engineering Model — A Status*** This paper will describe the development and status of the newest ORDEM model, ORDEM 4.0.
J.-C. LIOU, S. KAWAMOTO, R. CORSARO, M. ORTIZ, *ET AL.*	***The Multi-layer Acoustic & Conductive-grid Sensor (MACS) Technology Demonstration on HTV-X3*** This paper provides a summary of the rationale, MACS technology development, and preparation for the upcoming HTV-X technology demonstration mission.

CONFERENCE ABSTRACTS FROM THE NASA HVIT GROUP

The 9th European Conference on Space Debris, 1-4 April 2025, Bonn, Germany

Authors	Abstract Title and Summary
J. HYDE, D. LEAR, AND C. CLINE	***MMOD Risk to the International Space Station and its Sensitivity to Particle Size*** Along with describing the process of running this analysis through the Bumper code, this paper will provide the MMOD failure results and risk distribution details for the breakdown of the risk from both meteoroids and orbital debris, inclusive of all density bins included in each respective environment model. A direct comparison of MMOD risk for Russian and US segments will be provided, including the relevant ballistic limit equations and critical particle sizes.
C. CLINE, B. DAVIS, B. RENENDEZ, AND T. ASTON	***Evaluating Basalt Fabric in Stuffed Whipple and Multishock Shields Through Comparative Hypervelocity Tests*** This paper will present a testing campaign to explore the relative performance of basalt fabric in substitution for Nextel™ in two common MMOD shields, the Stuffed Whipple, and the multishock.

UPCOMING MEETINGS

5-9 May 2025: 5th Applied Space Environments Conference (ASEC), League City, Texas, USA

The 5th Applied Space Environments Conference (ASEC) will be hosted by Space Weather Solutions and provides an opportunity for space environment engineers and applied space scientists to work together on solving complex challenges as they relate to crewed and robotic space missions. The call for abstracts ended on 7 March 2025. More information on the conference is available at: https://spaceweathersolutions.com/asec2025/.

10-13 August 2025: 39th Small Satellite Conference, Salt Lake City, Utah, USA

The 39th annual Small Satellite Conference will be centered around the theme of "Reaching New Horizons. New orbit. Same mission." The proliferative demand from governmental, commercial, and academic stakeholders to have access to space was made possible through satellite research and technological advancements. This conference will delve into the innovations and collaboration from diverse stakeholders currently shaping the future of satellite capabilities. The call for abstracts ended on 4 February 2025. Conference information is available at https://smallsat.org/.

16-19 September 2025: 26th Advanced Maui Optical and Space Surveillance Technologies Conference (AMOS), Maui, Hawaii, USA

The technical program of the 26th Advanced Maui Optical and Space Conference (AMOS) will focus on subjects that are mission critical to space situational awareness. The technical sessions will include papers and posters on space debris; space situational/space domain awareness (SSA/SDA); SDA systems and instrumentation; astrodynamics; satellite characterization; space weather; and related topics. The abstract submission deadline was 3 March 2025. All presenters must present their work in-person, but virtual attendance options are available for non-presenters. Additional information about the conference is available at https://amostech.com/.

29 September-3 October 2025: 76th International Astronautical Congress (IAC), Sydney, Australia

The 76th International Astronautical Congress (IAC) will be hosted by the Space Industry Association of Australia (SIAA) in Sydney, Australia, with a theme of "Sustainable Space: Resilient Earth," from 29 September to 3 October 2025. The International Academy of Astronautics (IAA) Space Debris Committee will again organize the Space Debris Symposium during the IAC. Ten debris sessions are planned on topics such as debris detection and tracking, environment modeling, mitigation, remediation, sustainability, and policy. The abstract submission deadline was 28 February 2025. Additional details of the 76th IAC are available at: https://www.iac2025.org/. ♦

INTERNATIONAL SPACE MISSIONS
1 November 2024 – 31 January 2025

Intl.* Designator	Spacecraft	Country/ Organization	Perigee Alt. (KM)	Apogee Alt.(KM)	Inc. (DEG)	Addl. SC	Earth Orbital R/B	Other Cat. Debris
1998-067	ISS dispensed objects	Various	425	420	51.6	5	0	1
2024-198A	DSN-3	JPN	35781	35793	0.1	0	1	0
2024-199A	IONOSFERA-M 01	CIS	815	818	98.8	54	0	0
2024-199B	IONOSFERA-M 02	CIS	816	817	98.8			
2024-200A	DRAGON CRS-31	US	414	417	51.6	0	0	1
2024-201B	PROTOSAT-1	RWA	609	624	97.9	0	0	2
2024-202A	STARLINK-32362	US	443	445	43.0	22	0	0
2024-203A	OBJECT A	PRC	507	527	97.5	3	1	0
2024-204A	STARLINK-11402	US	359	360	53.2	19	0	0
2024-205A	OBJECT A	PRC	514	543	97.5	14	1	0
2024-206A	KOREASAT 6A	SKOR	35782	35793	0.0	0	1	0
2024-207A	STARLINK-32303	US	469	470	43.0	23	0	0
2024-208A	HAIYANG 4A	PRC	649	652	98.0	0	1	1
2024-209A	STARLINK-11407	US	342	343	53.2	10	0	0
2024-210A	STARLINK-32499	US	442	446	43.0	23	0	0
2024-211A	TIANZHOU 8	PRC	389	393	41.5	0	1	3
2024-212A	ADS-01	AUS	35783	35791	0.0	0	1	0
2024-213A	STARLINK-11433	US	338	341	53.2	10	0	0
2024-214A	GSAT 20	IND	35778	35795	0.0	0	1	0
2024-215A	PROGRESS MS-29	CIS	413	416	51.6	0	1	0
2024-216A	STARLINK-32637	US	443	445	43.0	23	0	0
2024-217A	STARLINK-11465	US	340	342	53.2	19	0	0
2024-218B	SUPERVIEW NEO-2 03	PRC	505	508	97.4	0	1	0
2024-218C	SUPERVIEW NEO-2 04	PRC	506	508	97.4			
2024-219A	KINEIS-5C	FR	643	646	98.0	4	2	0
2024-220A	STARLINK-11384	US	356	357	43.0	22	0	0
2024-221A	GUANGCHUAN 01	PRC	491	505	50.0	0	1	0
2024-221B	GUANGCHUAN 02	PRC	492	505	50.0			
2024-222A	STARLINK-32311	US	442	446	43.0	23	0	0
2024-223A	KONDOR FKA NO.2	CIS	502	505	97.4	0	0	0
2024-224A	STARLINK-32529	US	443	445	43.0	23	0	0
2024-225A	USA 438	US	313	325	70.0	21	0	0
2024-226A	OBJECT A	PRC	993	1077	50.0	0	1	0
2024-226B	OBJECT B	PRC	1095	1113	50.0			
2024-227A	TJS-13	PRC	EN ROUTE TO GEO			0	1	0
2024-228A	HAISHAO 1	PRC	346	481	43.0	0	1	0
2024-229A	STARLINK-32686	US	469	471	43.0	23	0	0
2024-230A	COSMOS 2580	CIS	901	910	67.1	0	1	0
2024-231A	STARLINK-11394	US	359	360	53.2	19	0	0
2024-232B	QIANFAN-37	PRC	828	853	89.0	17	1	0
2024-233A	PROBA-3 CSC	ESA	644	60566	59.3	0	1	0
2024-233C	PROBA-3 OSC	ESA	650	60559	59.3			
2024-234A	SIRIUS XM-9	US	35760	35801	0.0	0	1	0
2024-235A	SENTINEL 1C	ESA	695	697	98.2	0	0	0
2024-236A	OBJECT A	IRAN	266	316	58.5	0	1	0
2024-236B	OBJECT B	IRAN	295	362	58.6			
2024-236C	OBJECT C	IRAN	159	177	58.5			
2024-237A	STARLINK-11496	US	335	338	43.0	22	0	0
2024-238A	GJZ 01	PRC	1089	1111	59.9	4	0	0
2024-239A	STARLINK-32648	US	446	448	53.2	21	0	0

continued on page 10

SATELLITE BOX SCORE

(as of 3 March 2025, cataloged by the U.S. SPACE SURVEILLANCE NETWORK)

Country/ Organization	Spacecraft*	Spent R/B & Other Cat. Debris	Total
CIS	1576	5221	6797
ESA	104	27	131
FRANCE	109	527	636
INDIA	113	85	198
JAPAN	207	99	306
PRC	821	4724	5545
UK	719	1	720
USA	9159	4829	13988
OTHER	1153	94	1247
Total	13961	15607	29568

* active and defunct

Visit the NASA
Orbital Debris Program Office Website
https://orbitaldebris.jsc.nasa.gov

Technical Editor
Chris Ostrom

Managing Editor
Ashley Johnson

Correspondence can be sent to:
Victoria Segovia
victoria.segovia@nasa.gov

National Aeronautics and Space Administration
Lyndon B. Johnson Space Center
2101 NASA Parkway
Houston, TX 77058

www.nasa.gov
https://orbitaldebris.jsc.nasa.gov/

INTERNATIONAL SPACE MISSIONS

1 November 2024 – 31 January 2025

continued from page 9

Intl.* Designator	Spacecraft	Country/ Organization	Perigee Alt. (KM)	Apogee Alt.(KM)	Inc. (DEG)	Addl. SC	Earth Orbital R/B	Other Cat. Debris
2024-240A	HULIANWANG DIGUI-01	PRC	1108	1129	86.5	9	0	0
2024-241A	PIESAT-2 09	PRC	524	527	97.5	0	0	0
2024-241B	PIESAT-2 10	PRC	520	526	97.5			
2024-241C	PIESAT-2 11	PRC	520	529	97.5			
2024-241D	PIESAT-2 12	PRC	525	526	97.5			
2024-242A	NAVSTAR 83 (USA 440)	US	20171	20195	55.0	0	0	0
2024-243A	USA 441	US	297	319	69.9	21	0	0
2024-244A	O3B MPOWER F7	SES	EN ROUTE TO OP. ORBIT			0	1	0
2024-244B	O3B MPOWER F8	SES	EN ROUTE TO OP. ORBIT					
2024-245A	TIANQI 33	PRC	892	903	45.0	0	0	0
2024-245B	TIANQI 34	PRC	894	901	45.0			
2024-245C	TIANQI 35	PRC	890	904	45.0			
2024-245D	TIANQI 36	PRC	888	900	45.0			
2024-246A	TJS-12	PRC	35782	35790	1.9	0	1	0
2024-247A	KORSAT-2	SKOR	NO ELEMS. AVAILABLE			27	0	1
2024-248A	STRIX 2	JPN	552	578	97.6	0	2	0
2024-249A	STARLINK-11444	US	335	338	43.0	20	0	0
2024-250A	RESURS P5	CIS	468	470	97.3	0	1	0
2024-251A	STARLINK-32702	US	446	448	53.2	21	0	0
2024-252A	ASTRANIS UTILITYSAT	UK	EN ROUTE TO GEO			0	1	0
2024-252B	NUVIEW ALPHA	UK	EN ROUTE TO GEO					
2024-252C	AGILA	UK	EN ROUTE TO GEO					
2024-252D	NUVIEW BRAVO	UK	EN ROUTE TO GEO					
2024-253A	SDX01	IND	458	476	55.0	0	0	0
2024-253B	SDX02	IND	458	476	55.0			
2024-253C	POEM 4	IND	326	341	55.2			
2024-254A	STARLINK-11518	US	335	338	43.0	20	0	0
2025-001A	THURAYA 4	UAE	EN ROUTE TO GEO			0	1	0
2025-002A	SJ-25	PRC	35549	36029	10.2	0	1	0
2025-003A	STARLINK-32713	US	443	445	43.0	22	0	0
2025-004A	STARLINK-11452	US	336	337	43.0	20	0	0
2025-005A	USA 463	US	281	290	70.01	21	0	0
2025-006A	STARLINK-11538	US	335	337	43.0	20	0	0
2025-007B	CENTISPACE-1 S7	PRC	628	654	55.0	9	1	1
2025-008A	STARLINK-11547	US	336	338	43.0	20	0	0
2025-009A	BUZZER-1	FR	508	520	97.4	110	0	0
2025-010A	BLUE GHOST	US	LUNAR SURFACE			0	1	1
2025-010B	HAKUTO-R	JPN	EN ROUTE TO LUNAR LANDING					
2025-011A	BLUE RING PATHFINDER	US	2423	19253	30.0	0	0	0
2025-012A	OBJECT A	PRC	516	529	97.5	0		
2025-012B	OBJECT B	PRC	515	528	97.5			
2025-012C	OBJECT C	PRC	515	528	97.5			
2025-012D	OBJECT D	PRC	515	527	97.5			
2025-013A	OBJECT A	PRC	527	546	97.6	0		
2025-013B	OBJECT B	PRC	531	551	97.6			
2025-013C	OBJECT C	PRC	528	547	97.6			
2025-013D	OBJECT D	PRC	528	547	97.6			
2025-013E	OBJECT E	PRC	528	547	97.6			
2025-014A	STARLINK-32806	US	359	361	43.0	22	0	0
2025-015A	STARLINK-33596	US	330	332	53.2	26	0	0
2025-016A	QIANFAN-55	PRC	1057	1081	89.0	17	1	0
2025-017A	TJS-14	PRC	EN ROUTE TO GEO			0	1	0
2025-018A	STARLINK-32883	US	304	306	53.2	22	0	0
2025-019A	STARLINK-11548	US	334	339	43.0	20	0	0
2025-020A	NVS-02	IND	185	37442	21.0	0	1	0
2025-021A	SPAINSAT NG1	SPN	EN ROUTE TO GEO			0	1	0

Intl. = International; SC = Spacecraft; Alt. = Altitude; Inc. = Inclination; Addl. = Additional; R/B = Rocket Bodies; Cat. = Cataloged
Notes: 1. Orbital elements are as of data cut-off date 31 January. 2. Additional spacecraft on a single launch may have different orbital elements. 3. Additional uncataloged objects may be associated with a single launch.